Available online at www.sciencedirect.com
ScienceDirect
Energy Reports 8 (2022) 370–379
www.elsevier.com/locate/egyr

The 5th International Conference on Electrical Engineering and Green Energy, CEEGE 2022, 8–11 June, Berlin, Germany

A super-sensitive metal object detection method for DD-coil-engaged wireless EV chargers by passive electromagnetic sensing

Songyan Niu[a,b], Shuangxia Niu[a,*], Cheng Zhang[b], Linni Jian[b,*]

[a] *Hong Kong Polytechnic University, Kowloon, 999077, Hong Kong, China*
[b] *Southern University of Science and Technology, Shenzhen 518055, China*

Received 27 July 2022; accepted 6 August 2022
Available online 18 August 2022

Abstract

Metal object detection (MOD) is very important to guarantee the thermal safety of wireless charging systems for electric vehicles (EVs). Regarding the MOD methods based on passive sensing coils, most previous designs are targeted at the systems employing unpolarized coils, and the detection criteria are voltage-difference-based (VDB). Unfortunately, they are unsuitable for those employing DD coils due to the fundamental difference of field pattern. In addition, the VDB method has an inherent problem of low sensitivity. To fix these two problems, in this work, a set of field-oriented sensing coils is devised, which successfully realizes blind-zone elimination and super-high sensitivity. The arrangement of sensing coils accords with the pole-to-pole field distribution of DD coils to highlight the influence of MOs. The blind zone caused by the axial symmetry of the coupling field is removed by a non-symmetric patch coil. Moreover, a MOD mechanism with new criteria for MO identification is developed, which is the core of super-high sensitivity. Tested by ten positions where MOs might intrude using a 3 kW prototype, the optimized sensing coils can entirely remove the y-axis blind zones. The average sensitivity for the charging area reaches up to 16.

Peer-review under responsibility of the scientific committee of the 5th International Conference on Electrical Engineering and Green Energy, CEEGE, 2022.

Keywords: DD coil; Electric vehicle (EV); Inductive power transfer; Metal object detection (MOD); Sensing coils

1. Introduction

The rapid growth in electric vehicle (EV) markets has been seen in the last ten years globally. In this context, as an important support technology, advances have also been made in wireless electric vehicle charging (WEVC) from the aspects of technical performance and commercial competitiveness. Among various approaches of WEVC, inductive resonance is currently deemed to be of the highest maturity and practical value, which demonstrates a proper balance of power class, efficiency, and transmission range [1]. For the WEVC systems operated by this

* Corresponding authors.
E-mail addresses: eesxniu@polyu.edu.hk (S. Niu), jianln@sustech.edu.cn (L. Jian).

https://doi.org/10.1016/j.egyr.2022.08.122

Peer-review under responsibility of the scientific committee of the 5th International Conference on Electrical Engineering and Green Energy, CEEGE, 2022.

approach, a kind of thermal risk should be paid careful attention to, viz., metal objects (MOs). In practice, when MOs, such as a nail, coin, or gum wrapper, fall into the charging area inadvertently, they interact with the high-frequency coupling field magnetically and will be induced with eddy currents. As a consequence, the accumulated eddy-current losses can lead to quick and sharp temperature rises on the MO surface, which may ignite the objects of low combustion points such as dead leaves, impair the WEVC device, or even harm the living bodies [2].

To enable safe and stable WEVC, metal object detection (MOD) technology has been attracting more and more attention in recent years. MOD implementation can generally rely on physical sensors, system parameter analyzers, and auxiliary sensing coils. For the first method, available physical properties for MOD include temperature [3], infrared spectrum [4], hyperspectrum [5], and so forth. Today, this method has become less competitive due to high cost, low reliability (e.g., when a camera meets foggy weather), and low response time (e.g., temperature rises of MOs are not instant due to inertia). For the second method, the disturbance of MOs on the original coupling field will be manifested by the system parameters, including the transmitted power losses [6], primary frequency deviation [7], fifth-order harmonic current [8], and so forth. Herein, the significant attractions lies in low cost and complexity. However, this method is less suitable for WEVC systems, a kind of high-power application, since the degree of parameter change by MOs is usually too slight to be detected. For the third method, the above-mentioned distortion of the coupling field can be quantified by either the terminal voltage or impedance of sensing coils. The resultant change of these two parameters by MOs can be significant. Therefore, this method is particularly feasible for WEVC systems of high power level and our discussion will be based on it in the following.

The MOD methods by sensing coils mainly refer to those are voltage-difference–based (VDB). In [9], the concept of the VDB is introduced for the first time. The basic detection principle states that, the induced voltages of two symmetrical sensing coils cancel with each other in the absence of MOs, while their differences will deviate from zero once MOs intrude. However, if any MO locates in their intersection area, the voltage difference remains zero as usual, leading to fault MOD results. This area is called the blind zone, the biggest pain point deteriorating MOD accuracy. Regarding blind-zone elimination, substantial efforts have been made to optimize the topology and arrangement of sensing coils. The proposed novel MOD schemes include double-layer coil structure [10], interleaved coil connection in critical field region [11], s-shaped array coils [12], and so forth. By conducting a detailed review of these literatures, it is found that the effectiveness of corresponding designs is verified by unpolarized coupling coils without exception. In fact, WEVC systems with DD-coil-coupling engaged is also commonly used in practice with the virtue of a larger charging zone and a higher power level. As is known, the field pattern of unpolarized coils (e.g., rectangular coils) and polarized ones (e.g., DD coils) is fundamentally different [13,14]. In light of this, an open and interesting question is emerging: can the existing passive MOD schemes for WEVC systems with rectangular coils also apply to those employing DD coils?

Unfortunately, the answer is no. This judgment is verified in [15] by quantitative analysis. To bridge the gap, a set of sensing coils with novel size-modulated c-shape coil units achieving blind-zone-free purpose is proposed, which is specifically targeted at WEVC systems with DD coils involved [15]. Nevertheless, as a VDB design, it is inherently less sensitive since the voltage variation incurred by MO intrusion is much smaller compared with the voltage induced by the coupling field originally. In this paper, a super-sensitive MOD method is proposed without sacrificing cost-effectiveness. From the aspect of coil design, the pole-to-pole field distribution characteristics of DD coils are artfully utilized, which is distinctly different from those employ field symmetry. From the aspect of data sampling and processing, the criteria that whether MOs exist is changed from the voltage difference of a sensing coil pair to the individual voltage of each sensing coil. This new detection mechanism is featured by a theoretically zero-value voltage in the absence of MOs, which is the key to realizing super-high sensitivity.

2. Design of high-sensitivity sensing coils

2.1. Topology design

The topology of the proposed pole-to-pole coils is depicted in Fig. 1. Overall, these sensing coils are shaped in the form of rectangular channels, distributed along the y-axis, installed above the transmitting (Tx) pad of the WEVC system, and fully cover the Tx surface. This set of sensing coils comprises n channels with a multi-turn coil arrangement for sensitivity enhancement. This coil design is oriented by the field characteristics of DD coils, which are shown in Fig. 1(a). As can be observed, the coupling field between the Tx and receiving (Rx) side is very concentrated, symmetric about the y-axis, and exhibits a C-shape pattern (pole-to-pole). These enable that,

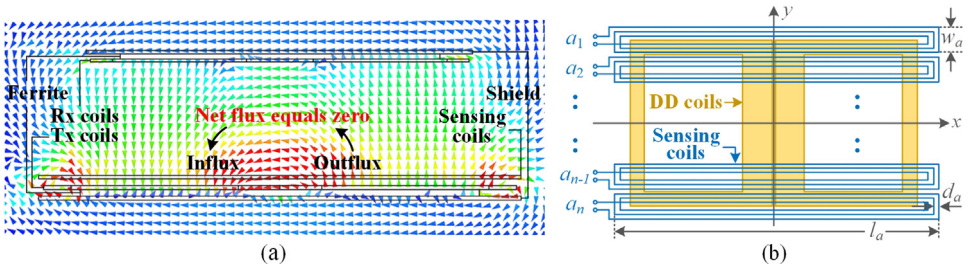

Fig. 1. Field-oriented design of sensing coils. (a) Field distribution of DD coils. (b) Topology of sensing coil.

seen from the xy-plane of sensing coils, the total amount of influx and outflux is equal. In other words, the net flux is zero, which results in a zero voltage in each sensing coil channel. Only when a MO intrudes the charging area and distorts the original coupling field, an imbalance emerges between the influx and outflux, the induced voltage evidently deviates from zero, and therefore the intruded MO can be detected.

Fig. 2 illustrates the distortion of the coupling field arising from an intruded MO by taking a 330-mL aluminum can as an example. For the whole coupling field region, the field symmetry is spoiled obviously. For the area enclosed by the aluminum can and its proximity, the intensity of the original field is reduced significantly due to the opposite polarity of the induced eddy current field. In addition, since the magnetic flux in these areas is largely vertical, the reduction effect is more potent in the y-direction. For the xy-plane of the pole-to-pole coils that should be focused specifically, the influx on the left is fairly more than the outflux on the right at this time point. The dominant influx is eventually embodied in a non-zero voltage of a sensing channel, which is a signal signifying the existence of MOs.

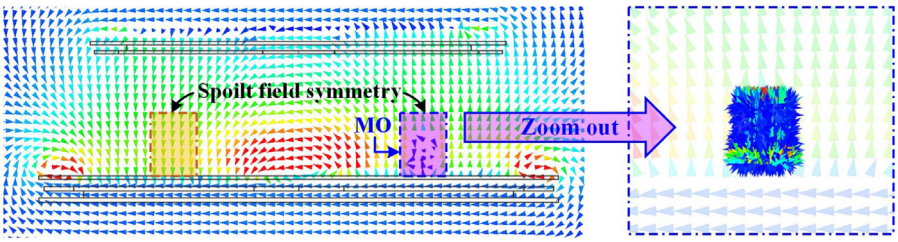

Fig. 2. Distortion of coupling field caused by an aluminum can.

As discussed above, the proposed MOD method is implemented on the premise of a zero voltage of sensing coils at the initial stage. To explain why this zero value can be stably and easily obtained in a quantitative manner, Fig. 3(a) gives the geometry of DD coils and sensing coils. Considering the sensing coils are arranged close to the Tx side, the DD coils on the Rx side can be safely neglected in this figure due to their negligible influence. As

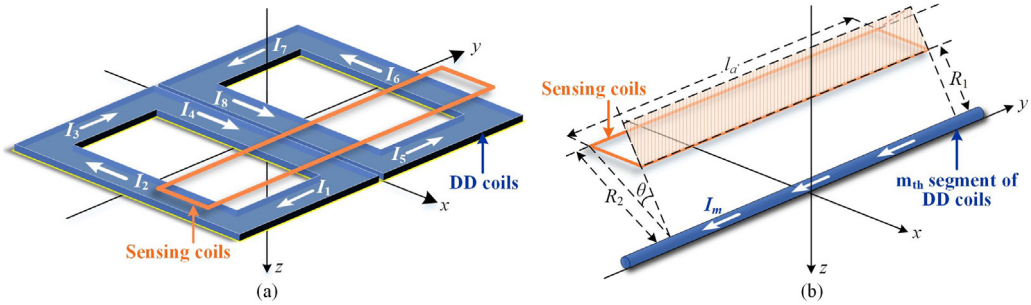

Fig. 3. Quantitative analysis of U_i. (a) Geometry of DD coils and sensing coils. (b) Calculation of $B_{z,m}$ using a line-loop model.

can be seen, the DD coils are divided into eight segments in all. In line with the superposition principle, the total induced voltage of a sensing channel U_i should be contributed by magnetic flux generated by these eight current sources, which is expressed as

$$U_i = \frac{d}{dt}\sum_{m=1}^{8}\varphi_m \quad for\, i = 1, 2, \ldots, n \tag{1}$$

where φ_m denotes the flux associated with the m_{th} current segment, and n is the number of sensing coils. The φ_m can be calculated using a line-loop model in Fig. 3(b), which states

$$\varphi_m = \int k\dot{B}_{z,m}dS = \frac{\mu_0\dot{I}_m}{2\pi}\int_{R_1}^{R_2\cos\theta}\frac{1}{r}adr \tag{2}$$

where $B_{z,m}$ denotes z-axis magnetic flux density of the m_{th} current segment in space, I_m is the current flowing through each segment, k describes the degree of how ferrite core intensifies the field density, and l_a is the length of sensing coils. Identified by (2), φ_1 and φ_5, φ_2 and φ_6, φ_3 and φ_7, and φ_4 and φ_8 can cancel with each other due to the opposite direction of the respective segment current. To sum up, the φ_m can be guaranteed a zero value regardless of time. Accordingly, U_i yields zero everywhere based on (1).

2.2. Sensitivity analysis

Sensitivity is a crucial MOD performance index in evaluating the ability of sensing coils to detect slight changes by MOs. In previous pieces of literature, it is usually defined as [16]

$$S_1 = \frac{\left|U_i' - U_i\right|}{U_i}\cdot 100(\%), \quad \text{for}\, i = 1, 2, \ldots, n \tag{3}$$

where U_i and U_i' are the terminal voltage of a sensing channel in the absence and presence of MOs, respectively. For conventional VDB methods, U_i can reach up to a few volts, while U_i' is merely hundreds of mV or even smaller. Therefore, it has been very demanding for S_1 to exceed 10%. In contrast, for the proposed MOD method herein, S_1 is infinite because U_i is theoretically zero. Although such a high S_1 seems very effective, it is actually not practical. For example, two sampled differences of U_i and U_i' are 10 mV and 100 mV, respectively. It is natural to understand that the latter definitely corresponds to a much better MOD performance. However, in view of S_1, they are the same.

To solve this problem, a modified sensitivity is developed and defined as

$$S_2 = \frac{U_i'}{U_{i,wom}}\cdot 100(\%), \quad \text{for}\, i = 1, 2, \ldots, n \tag{4}$$

where $U_{i,wom}$ represents the induced voltage of the i_{th} sensing coil without MOs. Note that, $U_{i,wom}$ should be theoretically zero as previously analyzed. However, in practice, this parameter can reach tens of mV mainly due to the extended coil terminals. Additionally, the imperfect field symmetry due to inevitable manufacturing errors is another factor contributing to the value of $U_{i,wom}$. The advantages of modified sensitivity include, firstly, the infinite sensitivity will no longer exist. Secondly, high-sensitivity characteristics can be maintained owing to the proposed new MOD mechanism, unlike the VDB method. Thirdly, the existence of MOs can be explicitly identified once S_2 is larger than 1. More precisely speaking, S_2 is several times more than 1.

As illustrated in Fig. 1(b), l_a, w_a, and d_a are three parameters determining the size of a sensing coil channel. Herein, the coil length l_a is fixed to be 200 mm to cover the whole Tx surface. The coil pitch d_a is set to 1 mm, a very small value, so that more magnetic flux can penetrate the sensing coils for sensitivity improvement [15]. As for the coil width w_a, the relationship between modified sensitivity S_2 and different values of w_a is described in Fig. 4(b). In case the determined w_a might not be suitable for some of all n sensing coils, three typical test positions are exemplified, covering over half of the Tx surface. According to (4), before jumping to sensitivity evaluation, $U_{i,wom}$ should be obtained in advance, which is exhibited in Fig. 4(a). The simulation results reveal that the induced voltage increases with w_a, but it is not linearly positive with w_a and has a gradually limited growth when w_a exceeds 18 mm. Moreover, 18-mm w_a performs the best in terms of modified sensitivity. Eventually, 18-mm w_a is selected.

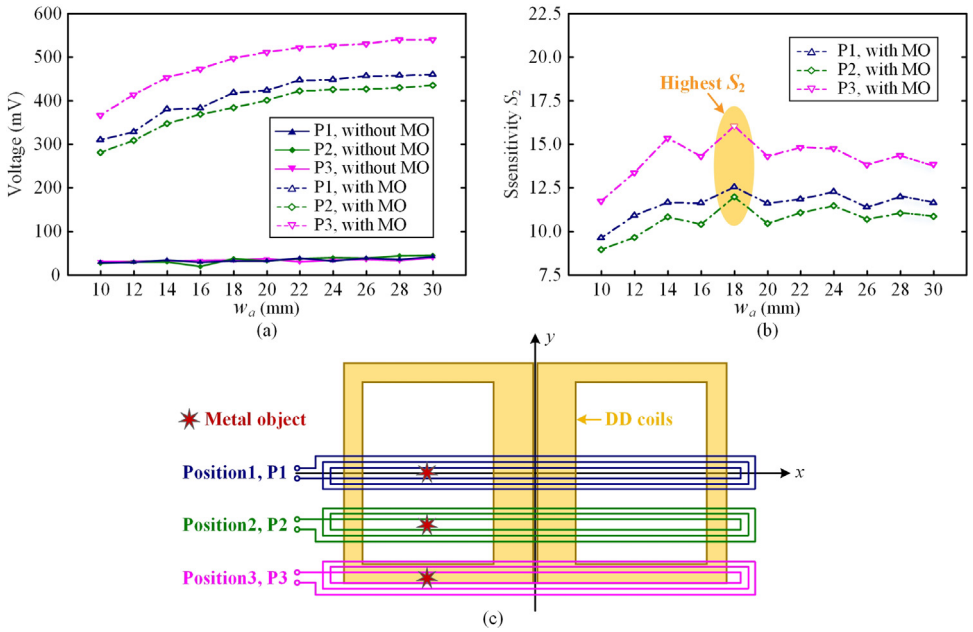

Fig. 4. (a). Determination of w_a. (a) Induced voltage of a sensing channel with different w_a. (b) Modified sensitivity S_2 with different w_a. (c) Test positions of sensing channels and metal objects.

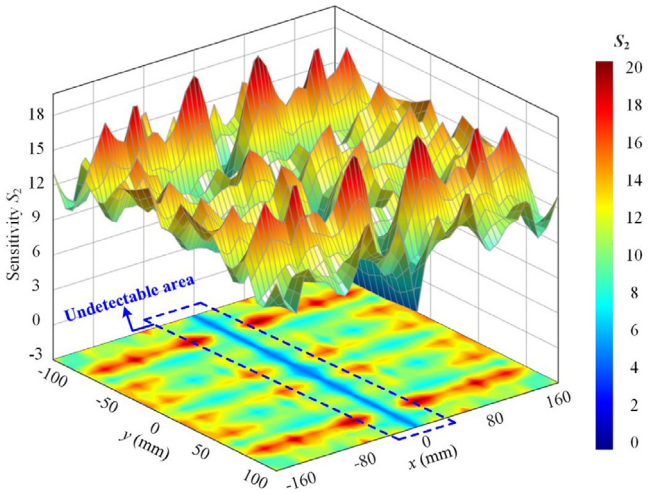

Fig. 5. Sensitivity distribution associated with different positions of MOs. (For interpretation of the references to color in this figure legend, the reader is referred to the web version of this article.)

In respect of the Tx surface, Fig. 5 exhibits the sensitivity distribution associated with various test points of a 330-mL can made of aluminum. Establishing the FE model in Maxwell, the simulation is carried out by depositing the MO row by row with a 10-mm step. The results reflect that, overall, the intruded MO can be detected in more than 90% of Tx surface if the sensitivity of 6 is set as the pass criteria. To be specific, the sensitivity of the area enclosed in blue in the y-axis ranges from 0.3 to 1.5, while that of other areas stably exceeds 6. This sensitivity characteristic can be explained by the eddy-current field flux in Fig. 6. When the MO appears in the y-axis, viz., x = 0 mm, the direction of generated eddy-current flux is largely parallel with no ability to penetrate the xy-plane of sensing coils. For the very limited vertical flux components, either the influx or outflux is not dominant. These characteristics are maintained despite the direction of the current I_{Tx}. In contrast, when the MO is distanced to the

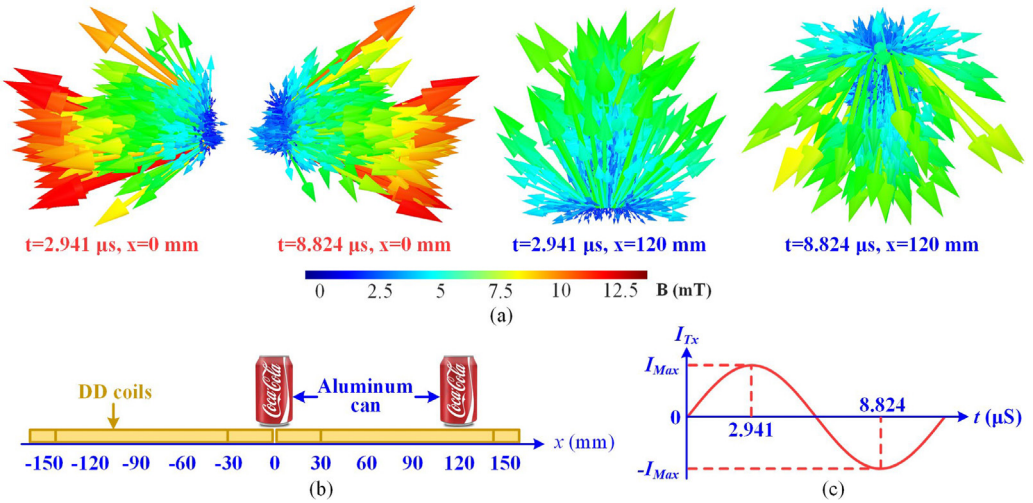

Fig. 6. Eddy-current field flux of an aluminum can intruding different positions in the charging area at different time points. (a) Flux distribution. (b) Test positions. (c) Test time points.

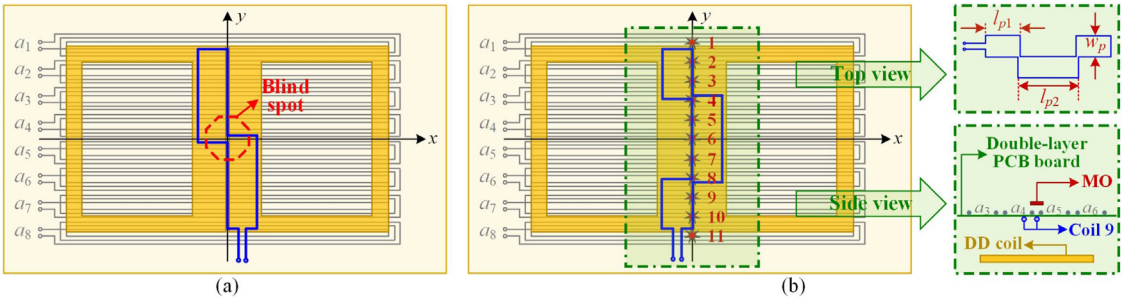

Fig. 7. Design of patch coil for blind-zone elimination. (a) Centrosymmetric coil. (b) Non-symmetric coil.

y-axis by 120 mm, there is always a dominant direction of vertical flux at different time points in a cycle. This necessitates blind-zone elimination, which will be detailed in Section 3.

3. Elimination of axial blind zone

To effectively remove the blind zone along the y-axis, an extra 9th coil, named patch coil, is devised in Fig. 7. Two versions of patch coil are proposed successively. As depicted in Fig. 7(a), the initial design consists of two rectangular units that are centrosymmetric. In MO's absence, the induced voltage of patch coil approximates zero since the magnetic flux penetrates one of the units and leaves away from the other. In the presence of MOs, the amount of net flux cannot remain zero with a terminal voltage standing out. Unfortunately, this working principle will be suddenly invalid once a MO appears in the central spot, which is enclosed by a red circle in Fig. 7(a). To ensure that a MO is able to influence the net flux amount directly even in this blind spot, an optimized non-symmetric coil is proposed, as shown in Fig. 7(b). Seen from the side view, this 9th coil and the other 8 coils are arranged on two sides of a PCB. Seen from the top view, the patch coil consists of three rectangular units. Two of them are shorter with the same length, while the third one is relatively longer so that an initial zero voltage can be obtained by flexible size modulation. For the blind spot of concern, the intruded MOs will simply change the flux density of the longer unit while the other two units are almost not affected. As a result, the induced voltage of the patch coil is changed from zero to a detectable value.

The parameters of the optimized patch coil to be studied include l_{p1}, $l_{p2,}$ and w_p. It should be noted that, the width of all three coil units is consistent for the convenience of size modulation. In other words, an initial zero

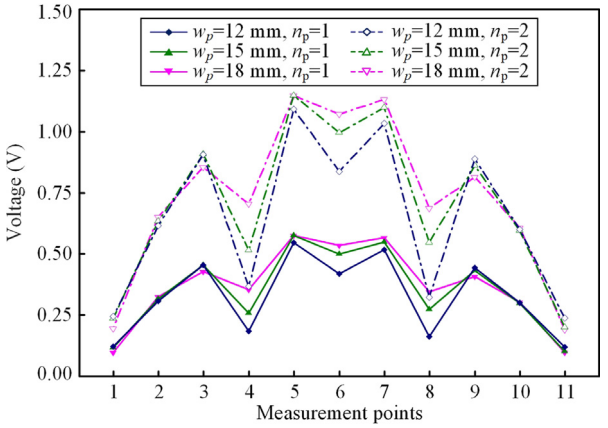

Fig. 8. Induced voltage of a patch coil with different w_p and n_p.

voltage is enabled by fixing w_p first and then adjusting l_{p1} and l_{p2} together. Three feasible combinations of these three parameters ($l_{p1}/l_{p2}/w_p$, unit: mm) state: 46/70/12, 45/72/15, 42/78/18. Due to the length limit of this paper, the sensitivity analysis for size modulation will not be elaborated.

As for the number of turns of patch coil n_p, alternative choices are 1 and 2, respectively. Such a small number of turns is selected to match the high-intensity magnetic field in the central area above DD coils. Based on different combinations of n_p, l_{p1}, $l_{p2,}$ and w_p, the simulation results of induced voltage are displayed in Fig. 8. Obviously, the voltage level corresponding to 12-mm and 15-mm w_p is smaller than that of 18-mm w_p. This is because the wider the width, the higher the proportion of vertical components of magnetic flux. Still, for sensitivity concern, the width of the patch coil is finally set to 18 mm. Based on the discussion in Section 2 and III, key geometry parameters of sensing coils are summarized in Table 1.

Table 1. Geometry parameters of sensing coils.

Parameter	Value	Parameter	Value	Parameter	Value
w_a (mm)	18	w_p (mm)	18	n_{a1} (i = 2,3,...,7)	3
l_a (mm)	20	l_{p1} (mm)	42	n_{a2} (i = 1,8)	2
d_a (mm)	1	l_{p2} (mm)	78	n_p	2

4. Results and discussion

To validate the effectiveness of the proposed super-sensitive sensing coils for MOD, a test bed has been established, as shown in Fig. 9. This test bed mainly includes a 3.0-kW charging system and a 345 mm × 247 mm

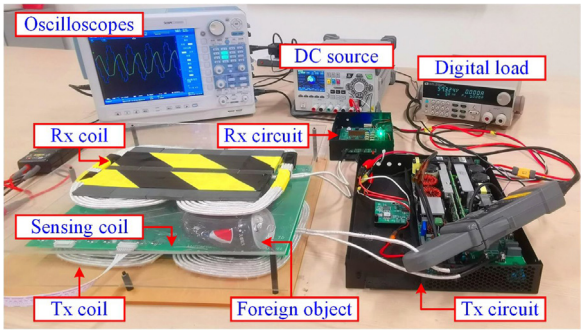

Fig. 9. Experimental test bed.

PCB for MOD use. The charging system comprises Tx and Rx DD coils electromagnetically coupled at a distance of 125 mm (normal position), and operates at 85.00 kHz as per SAE J2954. The LCL-S compensation is employed, which features an easy control of constant primary current independent of load variation. The MOD system mainly includes sensing coils and signal processing circuits with sampling resistors, LC filters, and operational amplifiers. The key parameters of this test bed are summarized in Table 2.

Table 2. Key parameters of test bed.

Parameter	Value	Parameter	Value
Output power (kW)	3.0	Tx coil inductance (μH)	89.57
Output dc voltage (V)	240	Rx coil inductance (μH)	87.84
Inverter current (rated) (A)	15	Air-gap length (mm)	100–150
Operating frequency (kHz)	85.00	Sensing coil size (mm)	320 × 200

To validate whether a MO can be detected in a super-sensitive manner with the blind zone removed by the proposed MOD scheme, an aluminum can of 330-mL volume is placed at 10 test points on the Tx surface in Fig. 10. The voltage signal is collected six times for each position to obtain an averaged value so that the sampling error and influence of variation of MO's temperature-dependent properties can be alleviated. Overall, this MO is detectable everywhere with an average sensitivity of higher than 16. Especially for the test points in proximity to the DD coil winding, the sensitivity reaches up to 45. More importantly, for the test points along the y-axis, viz., points 1–3, corresponding voltages all exceed 300 mV, which indicates a prominent difference compared with the no-MO status. In addition, the applicability of the proposed MOD scheme to different air-gap lengths is also verified. The results reveal that this Tx-side-installed MOD system is compatible with the EVs of different chassis heights.

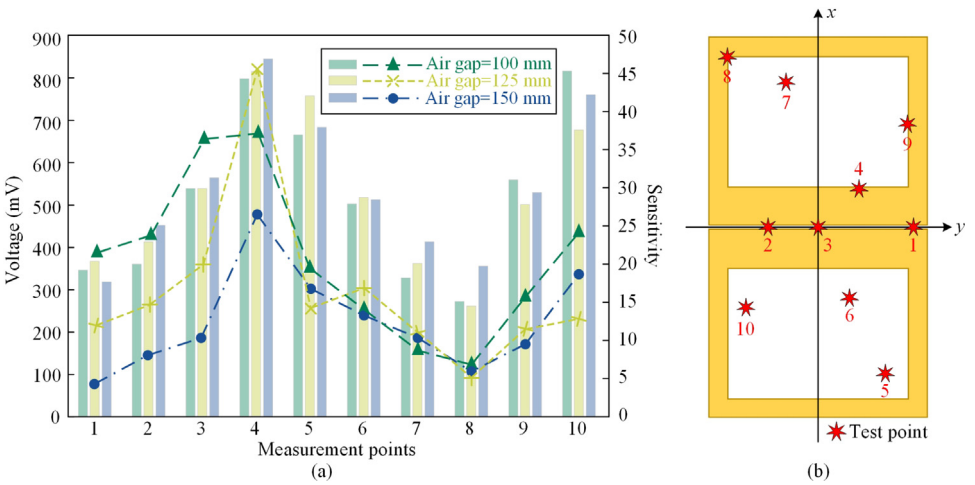

Fig. 10. Experimental results with different air-gap lengths. (a) Induced voltage and sensitivity. (b) Test positions for MO.

In practice, the charging area might be intruded by other types MOs, such as a coin or key. They not only have a smaller size but also lower conductivity than the aluminum can. Therefore, there is a practical possibility that they cannot be detected. In this regard, more strict experimental conditions are used to test the MOD performance of the proposed MOD scheme. For one thing, the selected MOs are much smaller. For another, the selected test points are only associated with the four lowest sensitivity in Fig. 10. The experimental results are given in Fig. 11. As can be observed, although the incurred voltages by a coin and key are lower than those of a can at each test point, they can safely exceed the counterpart without MOs. In a practical charging scenario, this is sufficient for MO identification. Even for the lowest voltage value, the sensitivity can reach 4.76.

5. Conclusion

Regarding the MOD methods based on passive sensing coils, there are mainly two challenges. For one thing, the existing coil designs which are targeted at WEVC systems by unpolarized-coil-coupling cannot be applied to those

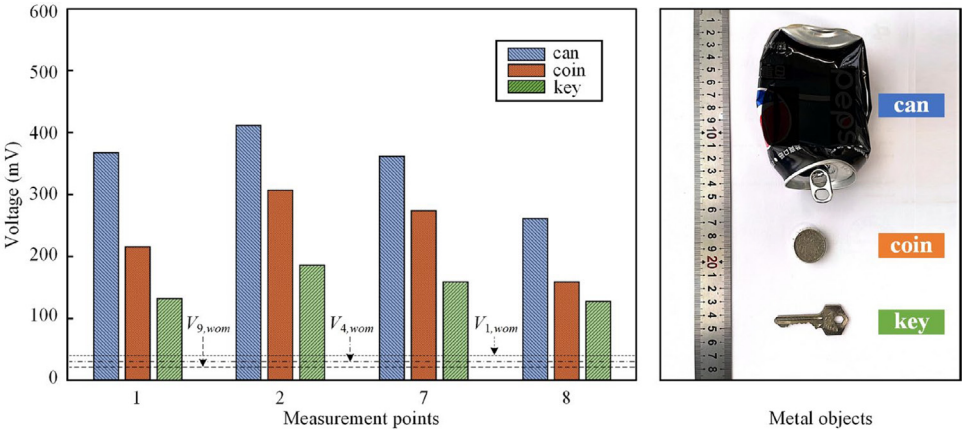

Fig. 11. Experimental results in low-sensitivity zone with different types of MOs.

by DD-coil-coupling. For another, low sensitivity is the inherent problem of conventional VDB methods. To bridge the gaps, in this work, a super-sensitive MOD scheme is proposed, which is highly accurate and reliable without sacrificing cost-effectiveness. To be specific, firstly, a set of field-oriented sensing coils, namely, pole-to-pole coils, are devised to magnify the influence of intruded MOs in the charging area. Secondly, a non-symmetric patch coil is proposed to remove the blind zones along the y-axis. Thirdly, a brand new MOD mechanism is developed, which is the core of super-high sensitivity. The criteria that whether MOs exist is changed from the voltage difference of a sensing coil pair to the individual voltage of each sensing coil. The effectiveness of the proposed MOD methods is validated using a 3-kW prototype with different air-gap lengths and various types of MOs. The selected MOs are stably detectable with an average sensitivity of 16 and a minimum of 4.76.

Declaration of competing interest

The authors declare that they have no known competing financial interests or personal relationships that could have appeared to influence the work reported in this paper.

Data availability

No data was used for the research described in the article.

Acknowledgments

This work was supported by the Science and Technology Innovation Committee of Shenzhen, China under project 20200925154042003.

References

[1] Niu S, Xu H, Sun Z, Shao Z, Jian L. The state-of-the-arts of wireless electric vehicle charging via magnetic resonance: principles standards and core technologies. Renew Sustain Energy Rev 2019;114(2019):109302.

[2] Luo X, Liu Z, Zhai H, Hou Y, Feng G, Li X. Optimized design of the detection coils for the metal foreign object detection system applied to wireless power transfer. Energy Rep 2022;8(2022):883–90.

[3] Sonnenberg T, Stevens A, Dayerizadeh A, Lukic S. Combined foreign object detection and live object protection in wireless power transfer systems via real-time thermal camera analysis. In: 2019 IEEE Applied power electronics conference and exposition. 2019, p. 1547–52.

[4] Kohmura A, Futatsumori S, Yonemoto N, Okada K. Optical fiber connected millimeter-wave radar for FOD detection on runway. In: 2013 European radar conference. 2013, p. 41–4.

[5] Tian Y, Li Z, Lin Y, Xiang L, Li X, Shao Y, et al. Metal object detection for electric vehicle inductive power transfer systems based on hyperspectral imaging. Measurement 2021;168:108493.

[6] Kuyvenhoven N, Dean C, Melton J, Schwannecke J, Umenei A. Development of a foreign object detection and analysis method for wireless power systems. In: 2011 IEEE Symposium on Product Compliance Engineering Proceedings. 2011, p. 1–6.

[7] Jafari H, Moghaddami M, Sarwat A. Foreign object detection in inductive charging systems based on primary side measurements. IEEE Trans Ind Appl 2019;55(6):6466–75.
[8] Long B, Zhu Q, Zang S, Zhao L, Hu A. Metal object detection by monitoring fifth-order harmonic current of IPT system with dual frequency tuning. IEEE Trans Power Electron 2021;37(3):2513–8.
[9] Simon V, Morris K, Katherine H, Lou H. Foreign object detection in wireless energy transfer systems. Patent U.S. 20130069441 A1. Watertown, MA: Witricity Corp; 2011.
[10] Xiang L, Zhu Z, Tian J, Tian Y. Foreign object detection in a wireless power transfer system using symmetrical coil sets. IEEE Access 2019;7(2019):44622–31.
[11] Thai V, Jang G, Jeong S, Park J, Rim C. Symmetric sensing coil design for the blind-zone free metal object detection of a stationary wireless electric vehicles charger. IEEE Trans Power Electr 2019;35(4):3466–77.
[12] Jeong S, Kwak H, Jang G, Choi S, Rim C. Dual-purpose nonoverlapping coil sets as metal object and vehicle position detections for wireless stationary EV chargers. IEEE Trans Power Electron 2017;33(9):7387–97.
[13] Budhia M, Boys J, Covic G, Huang C. Development of a single-sided flux magnetic coupler for electric vehicle IPT charging systems. IEEE Trans Ind Appl 2018;54(6):6383–93.
[14] Zhu G, Lorenz R. Achieving low magnetic flux density and low electric field intensity for a loosely coupled inductive wireless power transfer system. IEEE Trans Power Electron 2018;34(7):6062–75.
[15] Niu S, Niu S, Zhang C, Jian L. Blind-zone-free metal object detection for wireless EV chargers employing DD coils by passive electromagnetic sensing. IEEE Trans Ind Electron 2022. (2022, Early Access).
[16] Niu S, Zhang C, Shi Y, Niu S, Jian L. Foreign object detection considering misalignment effect for wireless EV charging system. ISA Trans 2022. (2022, Early Access).